Physical characterization of selenium nanoparticles and applications as anti-bacterial

Zainab Ali Hussain and Rasha Hamid Ahmed

Department of Physics, College of Education for Pure Sciences, Tikrit University, Tikrit, IRAQ

Abstract

Pulsed laser ablation in liquid (PLAL) is a technique that offers many advantages compared to traditional methods for preparing nanoparticles. A sample of pure selenium metal was used to synthesize nanoparticles using the pulsed laser ablation method in ethanol, employing an Nd:YAG laser with three pulse durations (20, 40, and 60) pulses at a wavelength of 1064 nanometers and an output energy of 240 mJ. This study examines the effects of varying the number of laser pulses on the properties of the resulting nanoparticles through structural and optical analysis, as well as their biological application. X-ray analysis indicated that selenium possesses a hexagonal crystalline structure, and the average crystal size decreases with an increase in the number of pulses. The results of the field emission scanning electron microscope indicated that the particle shapes were spherical and quasi-spherical, with some agglomerations appearing, while the average particle diameters decreased with an increase in the number of pulses. The optical properties showed improvement. The nanostructures of selenium showed significant antibacterial activity against both Gram-positive and Gram-negative bacteria.

Keywords: PLAL; Laser Pulse; Selenium nanoparticles; Bacteria.

Introduction

Nanostructured materials are excellent at mechanical, optical, electrical, biological, and chemical functions because they have a high surface area-to-volume ratio and quantum effects. Hence, they find use in a wide range of products. These products include catalysts, batteries, antibacterial agents, photo detectors, and solar cells, among others [1-4]. There are two established methodologies for synthesizing nanoparticles. Specifically, the top-down approach involves applying external forces on solid materials to fragment them into smaller particles [5]. We isolate the desired nanostructures from the main material by removing the substance [6]. The second method, known as the build-up or bottom-up strategy, involves layering the substrate with atoms one by one until molecules form [7]. Biosynthesis, also known as "green synthesis," is the process of using chemicals and living things (like plants, fungi, and bacteria) to turn oxidized selenium back into its elemental form. Physical techniques, such as pulsed laser ablation (PLAL), are also crucial for SeNP synthesis [8,9].

The reactions happen faster, there are fewer steps, no reducing agents are needed, labs are safer, and the nanoparticles are in the liquid phase [10]. This makes PLAL better than other methods in terms of safety, toxicity, and ease of extraction. This also makes the process eco-friendly. [10]. The chemical symbol for selenium is Se. It is not a metal and is in the same chalcogen group as oxygen, sulfur, and tellurium semiconductors in the third period of the periodic table. It possesses a mass of 78.963 Da. Electronic configuration: [Ar] 3d10 4s2 4p4 [11]. The melting temperature is 217°C [12]. Both pure selenium and nanomaterial's containing selenium exhibit semiconductor and biological activity qualities [13]. There is a wide range of uses for selenium nanoparticles, or SeNPs Inhibiting the proliferation of pathogenic bacteria and fungus is a capability of SeNPs Due to their small size and large surface area, selenium nanoparticles are able to cling to bacterial cell walls and destroy them [14].

2. Experimental Part

An Nd:YAG laser operating at a wavelength of 1064 nm, delivering an energy of 240 mJ, with a repetition rate of 6 Hz and a pulse duration of 9 ns, was employed to synthesize three solutions of colloidal nanoparticles in 5 ml of absolute ethanol, utilizing a pure selenium metal piece measuring 1×10×8 mm. The ethanol concentration was increased by 5 ml above the selenium target, and the distance from the laser source to the target was 12 cm. To assess the impact of augmenting the pulse count on the principal structural, optical, and biological characteristics of the synthesized colloidal solutions containing selenium nanoparticles, these properties were analyzed using X-ray diffraction (XRD), field emission scanning electron microscopy (FE-SEM), atomic force microscopy (AFM), and ultraviolet-visible spectroscopy. Additionally, antimicrobial efficacy.

XRD was used to determine, in addition to the crystalline structure, the average sizes of the prepared nanoparticles using the Debye–Scherrer's equation [15]:

$$D = \frac{K\lambda}{\beta \cos\theta} \text{.....(1)}$$

where K is the Scherrer constant, λ is wave length of the X-ray beam used (1.54184 Å). β is the Full width at half maximum (FWHM) of the peak and θ is the Bragg angle. FE-SEM was used to determine the morphology and average diameter of the prepared NPs, AFM was used

to determine the three-dimensional dimensions of nanoparticles (3D) and to analyze the overall scattering of sizes, topography, and distribution of nanoparticles. and Ultraviolet-visible spectroscopy was used to record the absorption spectra of the prepared nanoparticles and to calculate the absorptivity and transmittance, and the energy gap using the Tauc equation (2) [16].

$$\alpha h\upsilon = B\left(h\upsilon - Eg\right)^{\frac{1}{2}} \text{.....(2)}$$

where α is the absorption coefficient B is a constant, h is the Planck's constant, υ is the photon frequency, and Eg is the energy gap

3. Results and Discussion

3.1 XRD Analysis

X-ray diffraction (XRD) analysis of emulsified nanofluids synthesized using laser ablation at varying pulse rates (20, 40, and 60 pulses). X-ray diffraction (XRD) patterns reveal that SeNPs particles have three principal peaks for selenium at 23.873°, 30.107°, and 41°, as in Fig. (1). corresponding to the crystalline planes (100), (101), and (110) correspondingly. The results closely align with the data provided in card (ICDD.NO. 01-086-2244). Selenium displays a hexagonal crystal structure characterized by lattice constants a = b = 4.3000 Å and c = 4.8900 Å. The results indicated a rise in density corresponding to the escalation in the number of pulses (20, 40, and 60 pulses). The Scherrer equation was employed to ascertain the crystal size in equation (1). The augmentation in pulse frequency, while preserving a constant energy level, resulted in a notable enhancement in crystallization and a reduction in average crystal size from 133.6600127 nanometers to 80.50048667 nanometers, ultimately achieving 6.585382 nanometers [17]. Table (1) summarizes the results of XRD analysis.

3.2 FE-SEM Analysis

The FE-SEM analysis, as shown in figures (2), (3), and (4), using 20, 40, and 60 pulses, respectively, (a) shows the general morphology of the prepared samples on a scale of 1 micrometer and (b) a graph showing the distribution of the selenium nanoparticles, the particles exhibit spherical and semi-spherical shapes. With some agglomerations, we observe that the average diameter of the nanoparticles at 20 pulses was 54.72562 nanometers, at 40

pulses it becomes 45.9717 nanometers, and it becomes smaller at 60 pulses to 32.0214 nanometers. With the increase in the number of laser pulses, because the particles have aggregated and deposited on the surfaces of the target and the solution, the particles absorb the laser light, leading to their breakdown into smaller particles. As a result, the beam's power at the target decreases, and the amount of dissolved material does not increase further [18].

3.3 AFM Analysis

AFM analysis, as shown in figures (5), (6), and (7) using 20, 40, and 60 pulses, respectively, (a) a three-dimensional image and (b) a graph of the distribution of nanos selenium particles. The surfaces were smooth and of high quality, and the agglomerates had a uniform particle size and were nearly spherical. less leads to a reduction in particle size due to the ablation process. The evaporated laser beam interacts with the nanoparticles, limiting their size distribution [19]. The reduction in particle size is due to the phenomenon of laser ablation. The laser pulse stimulates the gradual fragmentation of large particles into smaller ones [20]. The roughness rate increases with the number of pulses [21].

3.4 Analysis of the absorption spectrum

Figure 8 illustrates the nanoparticles at different numbers of laser pulses. The absorption spectra vary with wavelength. Absorption is higher at shorter wavelengths (ultraviolet range) and decreases significantly at longer wavelengths. This means that the material absorbs less light in the visible and near-infrared ranges, making it easier to use as a window in solar cell technology. The number of laser pulses increases absorption compared to the lowest number of pulses, resulting in the removal of more material [22]. The absorption values were determined at a wavelength of 265 nm, as presented in Table 2.

3.5 Analysis of the Transmittance Spectrum

Figure 9, which shows how the transmittance spectrum changes with the wavelength for different numbers of laser pulses. It shows that transmittance inversely correlates with absorption in the electromagnetic spectrum, increasing with longer wavelengths in the ultraviolet region and sharply decreasing with shorter wavelengths. The concentration of absorbed nanoparticles in the solution increases with the number of laser pulses used. This makes the solution less transparent because the nanoparticles absorb more electromagnetic

radiation energy that strikes them [18]. The transmittance values were measured at a wavelength of 265 nanometers, as indicated in Table 2.

3.6 Analysis of the optical energy gap

The forbidden energy gap was found using the formula (2). Figure (10) shows the connection between photon energy and the change in $(\alpha h\nu)^2$. Increasing the number of laser pulses causes the energy gap to decrease. The increased number of photons reaching the material due to an increase in the number of laser pulses could explain this drop. The energy gap narrows as the concentration of electrons and holes rises as a result of the material absorbing more light. The rearrangement of the substance's atomic distribution is another cause of the energy gap narrowing [23].

3.7 The efficacy of selenium nanoparticles (SeNPS) against microorganisms

Metallic nanoparticles have a big effect on killing bacteria. This is because they can release metal ions into solutions. These ions are small and have a lot of surface area compared to their volume. Therefore, they can interact closely with the membranes of microbes [24]. We made selenium (Se) colloidal solutions using Pulsed Laser Ablation in Liquid (PLAL) with different pulse counts (20, 40, and 60). We measured the sizes of the inhibition zones in the culture medium to see how well they stopped the growth of different types of bacteria. Also, Figures 11 and 12 show that the secondary selenium nanoparticles made with 20, 40, and 60 pulses are very good at killing the Gram-positive Staphylococcus epidermis bacteria. Klebsiella pneumoniae, a Gram-negative bacterium, had the strongest inhibitory effect at high pulse counts. This shows that more laser pulses lead to stronger inhibition. Table (3) demonstrates the diameters of bacterial inhibition. Gram-negative bacteria have a special portion of their cell wall called LPS. It creates a negatively charged region that nanoparticles find appealing. Conversely, Gram-positive bacteria only contain teichoic acid in their cell walls. It keeps nanoparticles from building up by spreading them along the molecular phosphate chain. The cell wall of a Gram-negative bacteria has lipopolysaccharides, lipoproteins, and phospholipids that work together to make a barrier that only lets large particles in. Consequently, nanoparticles are more effective against Gram-positive bacteria than Gram-negative bacteria, according to numerous studies. On the other hand, Gram-positive bacteria possess a cell wall consisting of porous structures. These structures include peptidoglycan and teichoic acid.

These structures allow foreign particles to enter cells and cause cell death. Nanoparticles are more likely to stick to Gram-positive bacteria than Gram-negative bacteria because the surface of their cell walls has a strong negative charge [25].

conclusions

The pulsed laser evaporation method works well for making nanoparticles, and the size and properties of the nanoparticles depend on the number of laser pulses used. As the number of pulses increases, both the grain size and particle size decrease, while absorbance increases and both permeability and energy gap decrease. The manufactured selenium nanoparticles are very effective in killing bacteria. They work better against Gram-positive bacteria compared to Gram-negative bacteria.

References

[1] G. Schmid, Nanoparticles: From Theory to Application, 2nd ed., John Wiley & Sons, 2011.

[2] V. J. Mohanraj and Y. J. Chen, “Nanoparticles—A review,” Trop. J. Pharm. Res., vol. 5, no. 1, pp. 561–573, 2006.

[3] P. Holister, J. W. Weener, C. Roman, and T. Harper, “Nanoparticles,” Technol. White Papers, vol. 3, pp. 1–11, 2003.

[4] S. Hasan, “A review on nanoparticles: Their synthesis and types,” Res. J. Recent Sci., vol. 2277, p. 2502, 2015.

[5] F. M. Abdullah, A. M. Al-Ahmari, and S. Darwish, “Applications of nanoparticles via laser ablation in liquids: A review,” in Proc. Int. Conf. Ind. Eng. Oper. Manage., Bangkok, Thailand, Mar. 5–7, 2019.

[6] K. A. Mohammed, Preparation and Characterization of Nanogold by Laser Ablation, M.Sc. thesis, Faculty of Science, University of Kufa, 2016.

[7] S. A. Davari, An Experimental and Computational Investigation into Laser-Based Synthesis and Spectrochemical Characterizations of Metal/Intermetallic Nanoparticles with Engineered Interfacial Functionalities, Ph.D. dissertation, Univ. Tennessee, 2018.

[8] B. Hosnedlova et al., “Antioxidant properties and biomedical applications of selenium nanoparticles,” Int. J. Nanomedicine, vol. 13, pp. 2107–2123, 2018.

[9] S. Skalickova et al., “The role of selenium nanoparticles in nutrition and health,” Nutrition, vol. 33, pp. 83–90, 2017.

[10] G. Yang, “Laser ablation in liquids: Applications in the synthesis of nanocrystals,” Prog. Mater. Sci., vol. 52, pp. 648–698, 2007.

[11] W. C. Butterman and R. D. Brown, Mineral Commodity Profiles – Selenium, U.S. Geological Survey, p. 20, 2004.

[12] W. C. Cooper and R. A. Westbury, “Selenium,” in Selenium, R. A. Zhingaro and W. C. Cooper, Eds., Van Nostrand Reinhold, New York, p. 16, 1974.

[13] F. Jiang, W. Cai, and G. Tan, “Facile synthesis and optical properties of small selenium nanocrystals and nanorods,” Nanoscale Res. Lett., vol. 12, no. 1, p. 401, 2017.

[14] H. Kong et al., “Synthesis and antioxidant properties of gum arabic-stabilized selenium nanoparticles,” Int. J. Biol. Macromol., vol. 65, pp. 155–162, 2014.

[15] L.E. Smart and E.A. Moore, **“Solid State Chemistry: An Introduction”**, 3rd ed., Taylor & Francis, (2005), p. 105.

[16 J. Singh, **“Optical Properties of Materials and Their Applications”**, 2nd ed., John Wiley & Sons Ltd. (2020), p. 69.

[17] M. M. A. Al-Mousawi, Studying the Effect of the Number of Laser Pulses on the Structure, Morphology, and Optical Properties for a Thin Film of GO-Ag Nanocomposites, M.Sc. thesis, Univ. Babylon, College of Sciences for Women, Iraq.

[18] E. T. Salim and H. H. Rashed, “Laser pulses effect on the structural and optical properties of ZnO nanoparticles prepared by laser ablation in water,” Eng. Technol. J., vol. 32, no. 2, pp. 198–207, 2014.

[19] N. G. Semaltianos et al., “Silicon nanoparticles generated by femtosecond laser ablation in a liquid environment,” J. Nanoparticle Res., 2009.

[20] N. V. Tarasenko, V. S. Burakov, and A. V. Butsen, “Laser ablation plasmas in liquids for fabrication of nanosize particles,” Publ. Astron. Obs. Belgrade, vol. 82, pp. 201–211, 2007.

[21] N. Yasoob, N. J. Ghdeeb, N. H. Harb, and R. H. Jassim, “Study the morphological and optical properties of CdO doped ZnO thin films prepared by (PLD) technique,” J. Coll. Educ., vol. 1, no. 1, pp. 133–146, 2018.

[22] K. A. Aadim, S. J. Baadi, and A. K. Hussain, “Effect of laser energy and ablation time on the formation of aluminum nanoparticles by nanosecond laser ablation of an aluminum target in ethanol,” Iraqi J. Phys., vol. 12, no. 25, pp. 123–126, 2014.

[23] D. S. Murali, S. Kumar, R. J. Choudhary, A. D. Wadikar, M. K. Jain, and A. Subrahmanyam, "Synthesis of Cu2O from CuO thin films: Optical and electrical properties," AIP Adv. 5, 2015.

[24] R. Jeyaraman et al., “Synthesis and antimicrobial activity of copper nanoparticles,” Mater. Lett., vol. 71, pp. 114–116, 2011.

[25] A. Sarwar, H. Katas, S. N. Samsudin, and N. M. Zin, "Regioselective sequential modification of chitosan via azide-alkyne click reaction: Synthesis, characterization, and antimicrobial activity of chitosan derivatives and nanoparticles," PLoS One, vol. 10, no. 4, p. e0123084, 2015

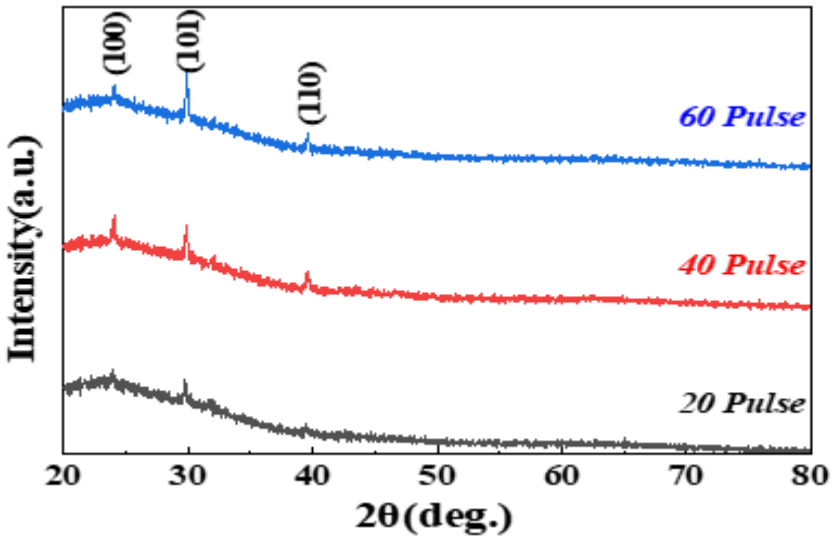

Fig. (1) The XRD pattern of Se NPs at different pulses

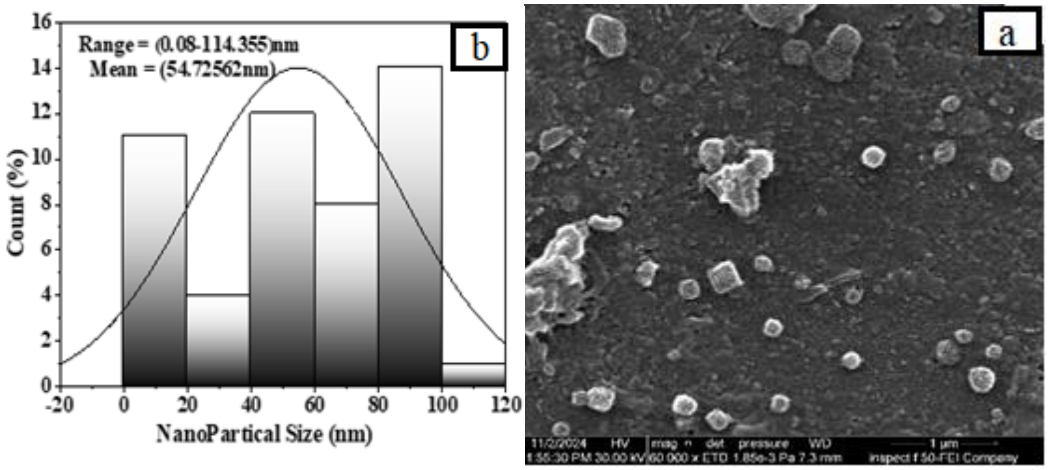

Fig. (2) FE-SEM images of prepared NPs using 20 pulse

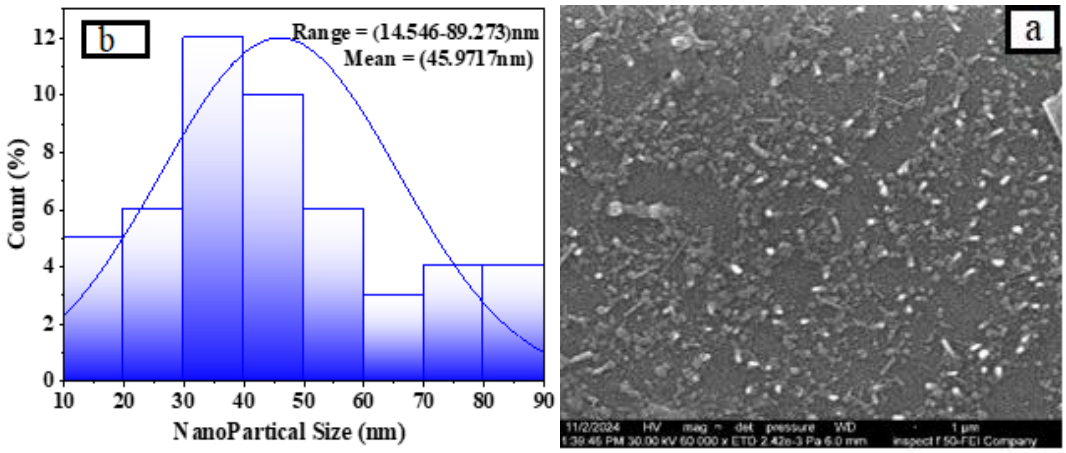

Fig. (3) FE-SEM images of prepared NPs using 40 pulse

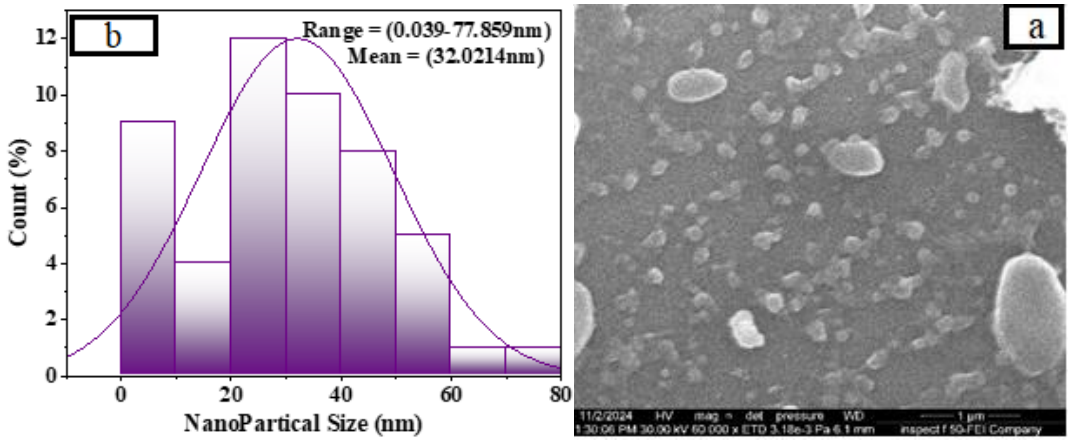

Fig. (4) FE-SEM images of prepared NPs using 60 pulse

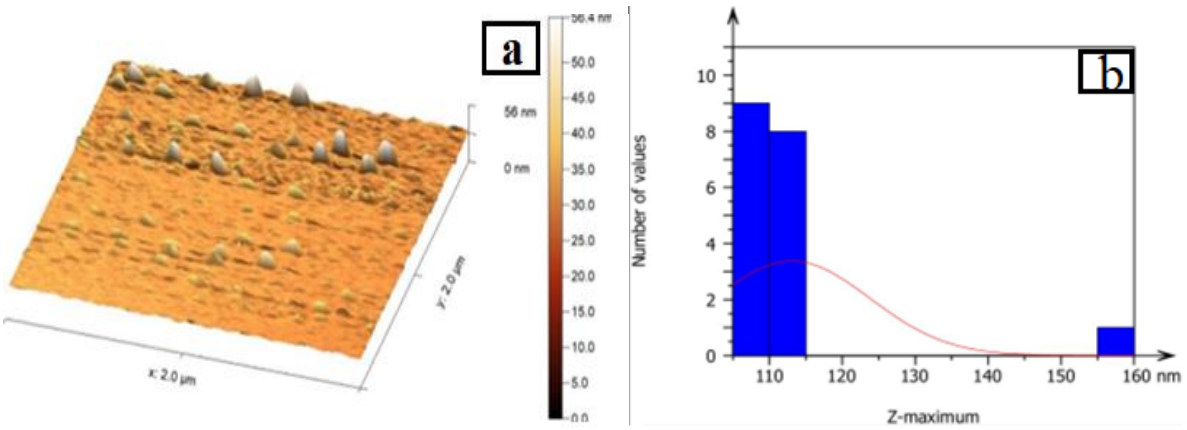

Fig. (5) AFM images of prepared NPs using 20 pulse

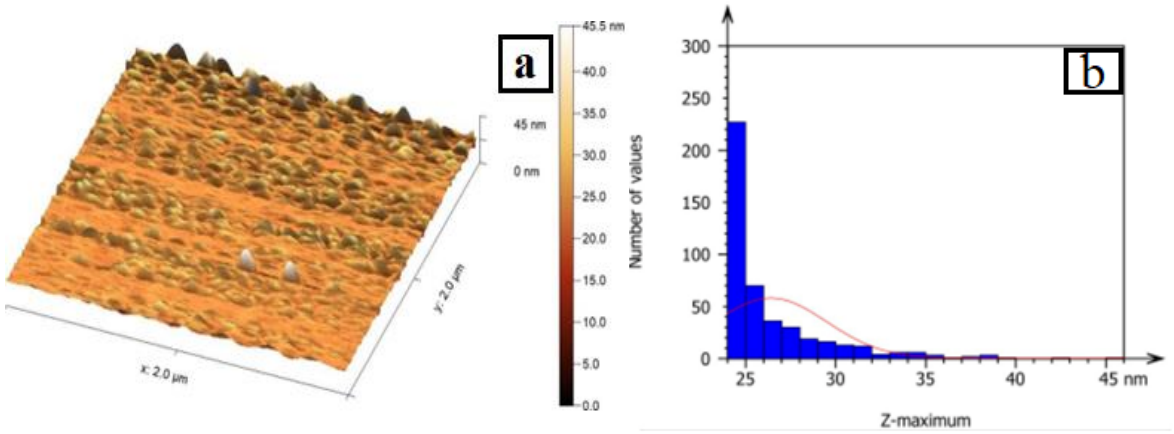

Fig. (6) AFM images of prepared NPs using 40 pulse

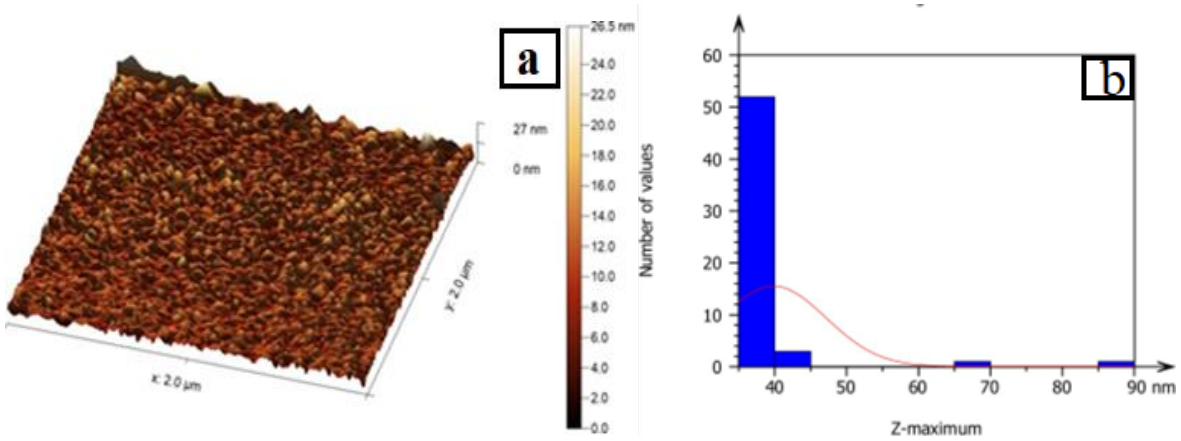

Fig. (7) AFM images of prepared NPs using 60 pulse

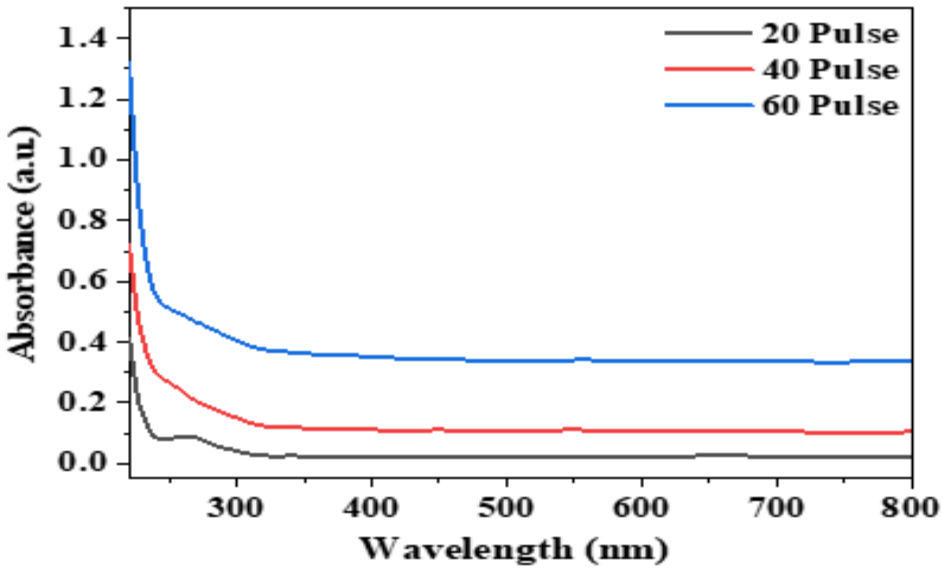

Fig. (8) Absorption spectra of selenium nanoparticles at different pulses

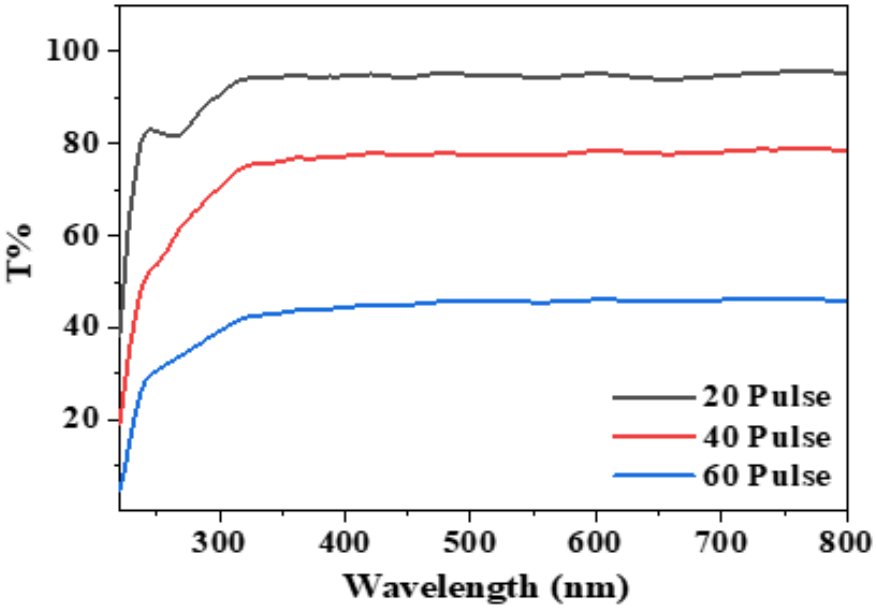

Fig. (9) Transmittance spectra of selenium nanoparticles at different pulses

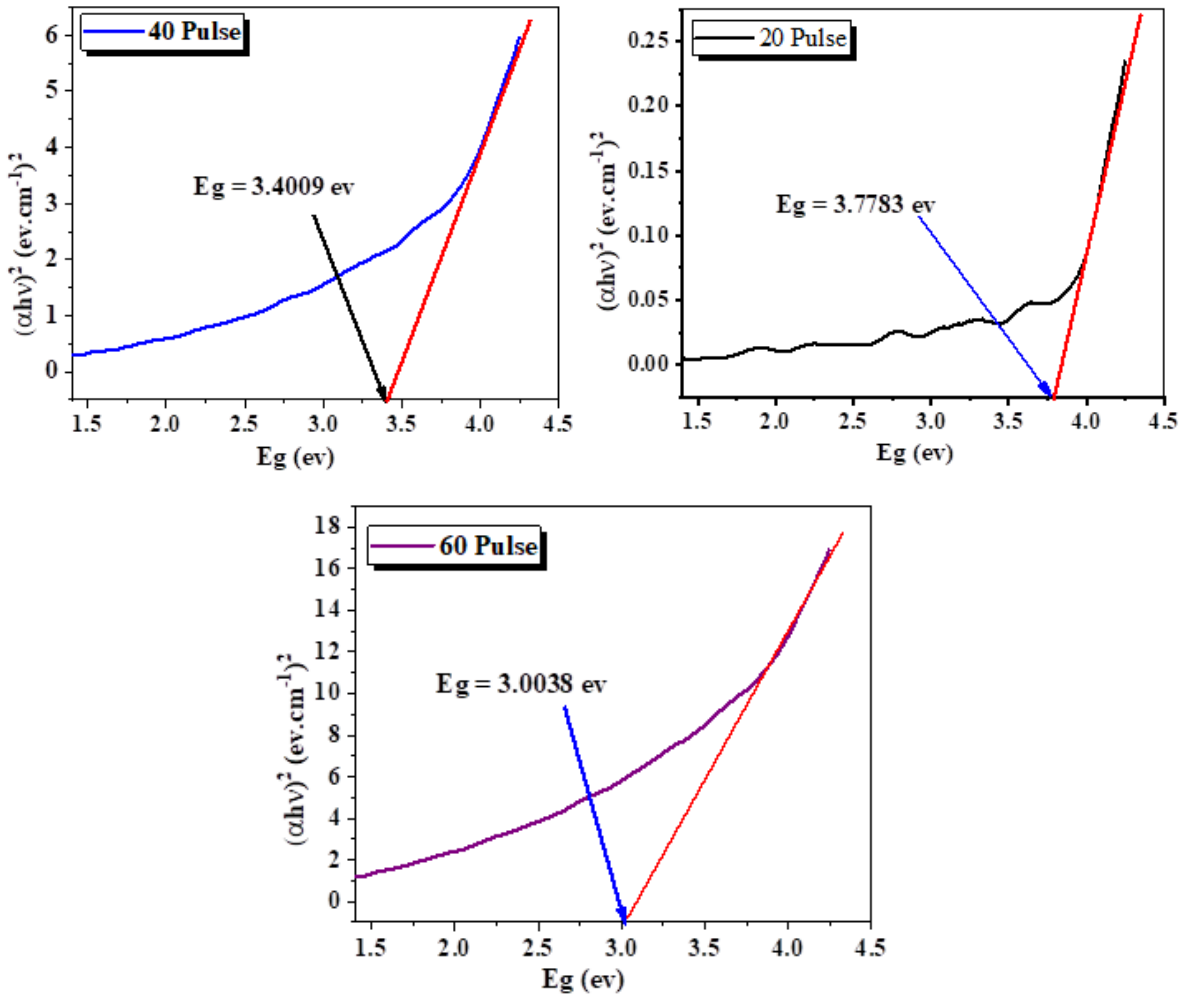

Fig. (10) Energy gap of selenium nanoparticles at different pulses

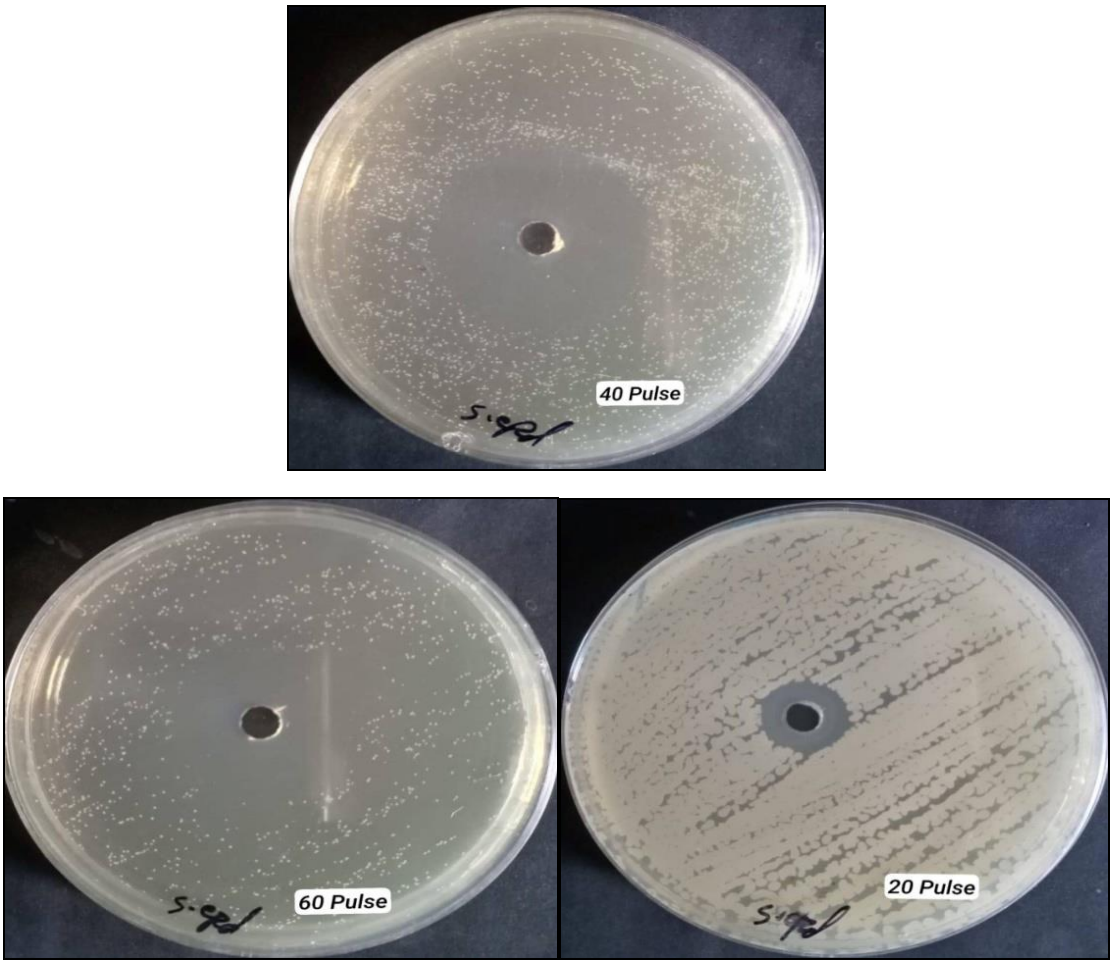

Fig. (11) Antibacterial activity against Staphylococcus epidermidis from selenium nanoparticles at different pulses

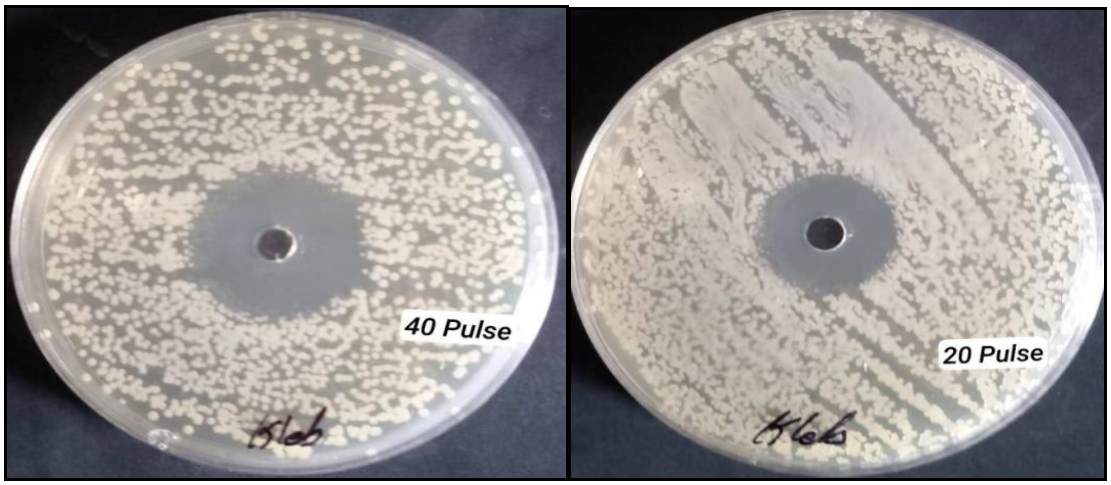

Fig. (12) Antibacterial activity against Klebsiella from selenium nanoparticles at different pulses

Table (1) XRD analysis results of prepared NPs

Pulse	2θ (deg)	FWHM (deg)	$d_{hkl}(A^{\circ})$	(hkl)	C.S (nm)	$C.S_{avg}$ (nm)	Card NO.
20	23.873	5.9424	3.7243	(100)	1.366428	133.6600127	01-086-2244
	30.107	0.6056	2.9666	(101)	13.58421		01-086-2244
	41.404	0.022	2.1788	(110)	386.0294		01-086-2244
40	23.5654	3.7588	3.7723	(100)	2.15901	80.50048667	01-086-2244
	29.7584	0.6541	2.9998	(101)	12.56675		01-086-2244
	41.0004	0.0374	2.1995	(110)	226.7757		01-086-2244
60	23.873	6.9741	3.7243	(100)	1.163632	6.585382	01-086-2244
	30.107	2.5207	2.9666	(101)	3.260964		01-086-2244
	41.404	0.5532	2.1788	(110)	15.33155		01-086-2244

Table (2) presents the values for absorbance and transmittance

Pulse	Absorbance	Transmittance
20	0.08835	0.81589
40	0.31683	0.48207
60	0.47416	0.33555

Table (3) displays the sizes at which bacteria are inhibited

Pulse	inhibition zone diameter (mm) (S.epd)	inhibition zone diameter (mm) (Kiebsiella)
20	16	20
40	27	23
60	36	30